J|A|C|S

ARTICLES

Published on Web 02/17/2007

$(I_2)_n$ Encapsulation inside TiO_2: A Way To Tune Photoactivity in the Visible Region

Sandro Usseglio, Alessandro Damin, Domenica Scarano, Silvia Bordiga, Adriano Zecchina,* and Carlo Lamberti*

Contribution from the Department of Inorganic, Physical and Materials Chemistry, NIS Centre of Excellence and INSTM Centro di Riferimento, Università di Torino, Via P. Giuria 7, I-10125 Turin, Italy

Received August 21, 2006; E-mail: adriano.zecchina@unito.it; carlo.lamberti@unito.it

Abstract: We report on the synthesis of nanovoid-structured TiO_2 material via a sol−gel route using titanium isopropoxide as precursor. The nanovoids are formed during the thermal treatment in air at 773 K. The surfaces of internal cavities are populated by the partial oxidation products of the organic part of the Ti precursor (CO_2, hydrogen carbonates, and residual isopropoxide groups). The thermal treatment in air at 773 K allows the maintainence, in the internal voids, of the encapsulated species. Addition of iodine in the synthesis procedure results in a new nanovoid-structured titanium oxide able to absorb light in the whole visible part of the electromagnetic spectrum. The origin of this absorption is attributed to the presence of $(I_2)_n$ adducts encapsulated in the nanocavities. These species coexist with partial combustion products of isopropoxide groups. Due to the protection of the TiO_2 walls, the $(I_2)_n$ adducts are not destroyed by thermal treatments in air. We have investigated whether the electron promoted in the excited state of the dye* molecule (upon absorption of visible light from the $(I_2)_n$ adducts) can be injected into either the TiO_2 conduction band or some titanium-localized acceptor, followed by migration of the injected electron to the surface where it reduces adsorbed organic molecules. Preliminarily experiments conducted with sunlight show that the surface-specific efficiency of this process, tested by following the degradation of methylene blue, is about 10 times higher than that of the P25 commercial TiO_2 photocatalyst.

1. Introduction

Among all the various semiconductors used in photocatalysis, TiO_2 is essentially the best material for environmental purification because of its many desirable properties.[1−5] Furthermore, the surface properties of TiO_2 are well-known because this solid has been widely investigated by a variety of physicochemical methods.[6−13] These facts, together with the cheap, readily available, nontoxic, photostable, and high oxidative power characteristics, make this solid ideal for characterization and photocatalytic studies. The initiation step of the photocatalytic process consists in the generation of electron−hole pairs upon irradiation of the material with a photon with energy at least equal to that of the band gap of the photocatalyst. The electron−hole pairs formed can either recombine in the bulk or travel up to the surface, where they can participate in chemical reaction species adsorbed on the external titanol groups. In this regard, TiO_2 combines two important, and generally antithetic, characteristics needed to improve the efficiency of a photocatalyst: (i) high surface area, needed to increase the number of external sites where photocatalytic reactions may occur; (ii) high crystalline quality, guaranteeing a low density of crystal defects where electrons or holes can be trapped. The last point is important because it implies a long mean free path of the electron−hole pair that, in turns, increases probability of transporting the charge carriers from bulk, where they are generated, to the surface, where they are used in the photocatalytic processes.

The only drawback of TiO_2 is that its band gap lies in the near-UV of the electromagnetic spectrum: 3.2 eV (285 nm) and 3.0 eV (410 nm) for anatase and rutile, respectively. As a consequence, only UV light is able to create electron−hole pairs and to initiate photocatalytic processes. As UV light constitutes only 5% of the solar spectrum,[14] 95% of the solar photons are useless for TiO_2 photocatalysts. It is therefore evident that any modification of the TiO_2-based photocatalysts resulting in a lowering of its band gap or in the introduction of stable optical sensitizes will represent a breakthrough in the field. For this purpose so many scientific works have appeared during recent

(1) Linsebigler, A. L.; Lu, G. Q.; Yates, J. T. *Chem. Rev.* **1995**, *95*, 735−758.
(2) Hoffmann, M. R.; Martin, S. T.; Choi, W. Y.; Bahnemann, D. W. *Chem. Rev.* **1995**, *95*, 69−96.
(3) Anpo, M.; Takeuchi, M. *J. Catal.* **2003**, *216*, 505−516.
(4) Chatterjee, D.; Dasgupta, S. *J. Photochem. Photobiol., C* **2005**, *6*, 186−205.
(5) Agrios, A. G.; Pichat, P. *J. Appl. Electrochem.* **2005**, *35*, 655−663.
(6) Carp, O.; Huisman, C. L.; Reller, A. *Prog. Solid State Chem.* **2004**, *32*, 33−177.
(7) Cerrato, G.; Marchese, L.; Morterra, C. *Appl. Surf. Sci.* **1993**, *70-1*, 200−205.
(8) Morterra, C. *J. Chem. Soc, Faraday Trans. 1* **1988**, *84*, 1617−1637.
(9) Diebold, U. *Surf. Sci. Rep.* **2003**, *48*, 53−229.
(10) Lana-Villarreal, T.; Rodes, A.; Perez, J. M.; Gomez, R. *J. Am. Chem. Soc.* **2005**, *127*, 12601−12611.
(11) Rego, L. G. C.; Batista, V. S. *J. Am. Chem. Soc.* **2003**, *125*, 7989−7997.
(12) Balachandran, U. G. E. N. *J. Solid State Chem.* **1982**, *42*, 276−282.
(13) Xamena, F.; Calza, P.; Lamberti, C.; Prestipino, C.; Damin, A.; Bordiga, S.; Pelizzetti, E.; Zecchina, A. *J. Am. Chem. Soc.* **2003**, *125*, 2264−2271.
(14) Yin, S.; Zhang, Q. W.; Saito, F.; Sato, T. *Chem. Lett.* **2003**, *32*, 358−359.

10.1021/ja066083m CCC: $37.00

years that an exhaustive analysis of the different approaches is beyond of scope of this contribution and only a selection of cases will be summarized below. (i) One case is doping TiO_2 with various transitions metals such as Au, Ag, Pt, Cr, Nb, V, Mn, and Fe.[3,6,15−18] These systems show an enhanced photoactivity in the visible with an efficiency depending highly on the preparation method. However, they are characterized by thermal instability and very critical is the control of the cluster dimension and distribution.[15] (ii) Another case is doping TiO_2 with nonmetals atoms such as N,[14,19,20] S,[21−28] F,[29] C,[20,30,31] I,[32] Br,[33] and Cl. [33] Also in this case the photocatalytic activity depends on the content of nonmetal atoms and on the method of preparation. (iii) A third case is anchoring a dye-sensitizer molecule on the surface of the photocatalyst.[4] Various dyes (catechol,[10] porphyrins,[34] phthalocyanines,[35] etc.) have been employed as sensitizer, but most of them are toxic and easily undergo a self-degradation process that makes them unsuitable for durable applications in photocatalysis.

The photocatalytic activity of microporous titanosilicates ETS-10 and ETS-4 has also been recently investigated.[13,36−41] Unfortunately, the fact that Ti atoms are organized in one-dimensional linear chains of TiO_6 octahedra (−O−Ti−O−Ti−), behaving as semiconducting nanowires,[42−46] causes a blue shift of the band gap. To overcome this drawback, Klabunde and co-workers[47] have introduced transition metal ions in ETS-10 either by addition of corresponding salts during the synthesis (Cr and Co samples with Cr (or) Co/Ti = 0.05) or by a postsynthesis ion-exchanged approach (Co and Ag).

The results of this study can be divided into three parts. In the first part we illustrate a new strategy to synthesize a titanium dioxide characterized by the presence of internal nanovoids. In the second part, we demonstrate that the walls of the internal cavities are populated by adsorbed molecular species derived form the partial combustion of isopropoxide groups. The formation mechanism of these species (which are stable to thermal treatments in air at 773 K, due to encapsulation) is discussed. In the third part we have evaluated the possibility to encapsulate, during the synthesis, a colored dye molecule such as iodine inside these nanocavities. The aim of this synthesis is to obtain a TiO_2 able to receive solar light for the presence of protected internal dye molecules and avoid in this way problems related to self-degradation and thermal instability.

To evaluate the crystalline phases and to control possible changes on the crystallinity and on the morphology before and after the iodine-doping treatments, X-ray powder diffraction (XRPD) and high-resolution transmission electron microscopy (HRTEM) have been applied. Raman and IR have been used to confirm the presence of nanovoids and to characterize the molecules present inside this cavities. UV−vis DRS allow us to evaluate the spectra of dye-sensitizer molecules present in the cavities. Finally to test the photoactivity of both the TiO_2 and the iodine-modified TiO_2 samples the degradation of methylene blue[26,48] (with sunlight) analyzed with UV−vis spectroscopy in transmission mode has been investigated and compared with the standard P25 TiO_2 commercial photocatalyst.

2. Experimental Section

2.1. Sample Preparation. TiO_2 powders were prepared by a sol−gel route using titanium isopropoxide ($Ti(OC_3H_7)_4$), which is liquid at ambient conditions, as precursor. A typical procedure for the synthesis of nanovoid-structured TiO_2 material (hereafter NVS-TiO_2) starts with the hydrolysis at room temperature of 3 g of $Ti(OC_3H_7)_4$ (purity 97% by Sigma-Aldrich) in air (30−40% humidity), hosted inside a beaker of 20 cm^2, according to eq 1:

$$Ti(OC_3H_7)_4 + 2H_2O \rightarrow TiO_2 + 4C_3H_7OH \qquad (1)$$

During hydrolysis, the liquid is kept under continuous stirring. After 36 h the white powder obtained was dried at 373 K in an oven and then calcined in air at 773 K for 6 h. When a larger amount of precursor was used or when a beaker of lower air/liquid surface is employed, a longer hydrolysis time is needed before starting the calcination. The material obtained after calcination at 773 K is a white powder; vide infra the left inset in Figure 5 or in the Table of Contents figure.

Among all possible dyes able to absorb photons of the visible light, iodine has been chosen because its high solubility in the used Ti precursor allows a straightforward synthesis. I_2-doped nanovoid-structured TiO_2 material (hereafter I_2/NVS-TiO_2) has been obtained by following the same procedure described for the NVS-TiO_2 material, the only difference in the synthesis being represented by the starting liquid obtained by dissolving 0.1 g of iodine crystal in 3 g of the (Ti-

(15) Choi, W. Y.; Termin, A.; Hoffmann, M. R. *J. Phys. Chem.* **1994**, *98*, 13669−13679.
(16) Wu, C. G.; Chao, C. C.; Kuo, F. T. *Catal. Today* **2004**, *97*, 103−112.
(17) Rodrigues, S.; Ranjit, K. T.; Uma, S.; Martyanov, I. N.; Klabunde, K. J. *Adv. Mater.* **2005**, *17*, 2467−2471.
(18) Kapoor, P. N.; Uma, S.; Rodriguez, S.; Klabunde, K. J. *J. Mol. Catal., A* **2005**, *229*, 145−150.
(19) Asahi, R.; Morikawa, T.; Ohwaki, T.; Aoki, K.; Taga, Y. *Science* **2001**, *293*, 269−271.
(20) Martyanov, I. N.; Uma, S.; Rodrigues, S.; Klabunde, K. J. *Chem. Commun.* **2004**, 2476−2477.
(21) Umebayashi, T.; Yamaki, T.; Itoh, H.; Asai, K. *Appl. Phys. Lett.* **2002**, *81*, 454−456.
(22) Umebayashi, T.; Yamaki, T.; Tanaka, S.; Asai, K. *Chem. Lett.* **2003**, *32*, 330−331.
(23) Ma, T. L.; Akiyama, M.; Abe, E.; Imai, I. *Nano Lett.* **2005**, *5*, 2543−2547.
(24) Di, Valentin, C.; Pacchioni, G.; Selloni, A.; Livraghi, S.; Giamello, E. *J. Phys. Chem. B* **2005**, *109*, 11414−11419.
(25) Livraghi, S.; Votta, A.; Paganini, M. C.; Giamello, E. *Chem. Commun.* **2005**, 498−500.
(26) Livraghi, S.; Paganini, M. C.; Giamello, E.; Selloni, A.; Di, Valentin, C.; Pacchioni, G. *J. Am. Chem. Soc.* **2006**, *128*, 15666 -15671.
(27) Ghicov, A.; Macak, J. M.; Tsuchiya, H.; Kunze, J.; Haeublein, V.; Frey, L.; Schmuki, P. *Nano Lett.* **2006**, *6*, 1080−1082.
(28) Batzill, M.; Morales, E. H.; Diebold, U. *Phys. Rev. Lett.* **2006**, *96*, 026103.
(29) Yamaki, T.; Umebayashi, T.; Sumita, T.; Yamamoto, S.; Maekawa, M.; Kawasuso, A.; Itoh, H. *Nucl. Instrum. Methods Phys. Res., Sect. B* **2003**, *206*, 254−258.
(30) Choi, Y.; Umebayashi, T.; Yamamoto, S.; Tanaka, S. *J. Mater. Sci. Lett.* **2003**, *22*, 1209−1211.
(31) Sakthivel, S.; Kisch, H. *Angew. Chem., Int. Ed.* **2003**, *42*, 4908−4911.
(32) Hong, X. T.; Wang, Z. P.; Cai, W. M.; Lu, F.; Zhang, J.; Yang, Y. Z.; Ma, N.; Liu, Y. J. *Chem. Mater.* **2005**, *17*, 1548−1552.
(33) Luo, H. M.; Takata, T.; Lee, Y. G.; Zhao, J. F.; Domen, K.; Yan, Y. *Chem. Mater.* **2004**, *16*, 846−849.
(34) Kalyanasundaram, K.; Gratzel, M.; Vlachopoulos, N.; Krishnan, V.; Monnier, A. *J. Phys. Chem.* **1987**, *91*, 2342−2347.
(35) Fan, F. R. F.; Bard, A. J. *J. Am. Chem. Soc.* **1979**, *101*, 6139−6140.
(36) Calza, P.; Paze, C.; Pelizzetti, E.; Zecchina, A. *Chem. Commun.* **2001**, 2130−2131.
(37) Howe, R. F.; Krisnandi, Y. K. *Chem. Commun.* **2001**, 1588−1589.
(38) Southon, P. D.; Howe, R. F. *Chem. Mater.* **2002**, *14*, 4209−4218.
(39) (a) Krisnandi, Y. K.; Southon, P. D.; Adesina, A. A.; Howe, R. F. *Int. J. Photoenergy* **2003**, *5*, 131−140. (b) Luca, V.; Osborne, M.; Sizgek, D.; Griffith, C.; Araujo, P. Z. *Chem. Mater.* **2006**, *18*, 6132−6138.
(40) Usseglio, S.; Calza, P.; Damin, A.; Minero, C.; Bordiga, S.; Lamberti, C.; Pelizzetti, E.; Zecchina, A. *Chem. Mater.* **2006**, *18*, 3412−3424.
(41) Krisnandi, Y. K.; Lachowski, E. E.; Howe, R. F. *Chem. Mater.* **2006**, *18*, 928−933.
(42) Borello, E.; Lamberti, C.; Bordiga, S.; Zecchina, A.; Otero, Arean, C. *Appl. Phys. Lett.* **1997**, *71*, 2319−2321.
(43) Lamberti, C. *Microporous Mesoporous Mater.* **1999**, *30*, 155−163.
(44) Bordiga, S.; Palomino, G. T.; Zecchina, A.; Ranghino, G.; Giamello, E.; Lamberti, C. *J. Chem. Phys.* **2000**, *112*, 3859−3867.
(45) Damin, A.; Xamena, F. X. L.; Lamberti, C.; Civalleri, B.; Zicovich-Wilson, C. M.; Zecchina, A. *J. Phys. Chem. B* **2004**, *108*, 1328−1336.
(46) Prestipino, C.; Solari, P. L.; Larnberti, C. *J. Phys. Chem. B* **2005**, *109*, 13132−13137.
(47) Uma, S.; Rodrigues, S.; Martyanov, I. N.; Klabunde, K. J. *Microporous Mesoporous Mater.* **2004**, *67*, 181−187.
(48) Zhang, T. Y.; Oyama, T.; Aoshima, A.; Hidaka, H.; Zhao, J. C.; Serpone, N. *J. Photochem. Photobiol., A* **2001**, *140*, 163−172.

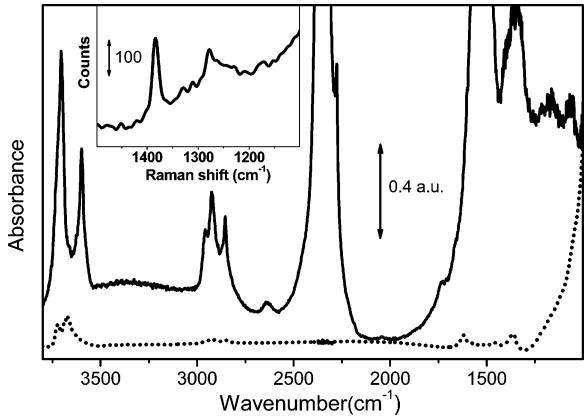

Figure 1. IR spectra of the NVS-TiO_2 sample (full line) and of P25 (dotted line) collected at room temperature after activation in vacuo at 773 K for 1 h. The inset reports, in the $\nu_{sym}(CO_2)$ stretching region, the Raman spectrum of the NVS-TiO_2 sample subjected to the same treatment. Note that, for experimental problems in the preparation of the pellets for in situ transmission IR, the thickness of the NVS-TiO_2 material is almost 10 times that of P25.

$(OC_3H_7)_4$) precursor. The surface area of the calcined materials resulted to be comprised in the 4.1−3.8 $m^2\ g^{-1}$ interval, independent of the presence of iodine dopant. These surface area are 1 order of magnitude lower than that of the Degussa P25 (60 $m^2\ g^{-1}$), frequently used for a standard TiO_2 photocatalytic experiment and also adopted here for sake of comparison.

With respect to the standard sol−gel procedures for TiO_2 preparation,[49] the main difference consists in the use of the Ti precursor as pure reagent, without diluting in alcohols. This peculiarity is important for the preparation of the I_2-doped TiO_2 material because it allows one to maximize the local joint density of Ti and I, a point that is crucial to maximize the amount of iodine encapsulated in the nanovoids of the TiO_2 material.

2.2. Characterization Techniques. The NVS-TiO_2 and the I_2/NVS-TiO_2 materials have been investigated by means of vibrational (IR and Raman) and optical (UV−vis in the DRS mode). XRD, TEM, and BET were used to characterize the structural morphology and texture. In particular FTIR spectra were collected, at 2 cm^{-1} resolution, in transmission mode on a Bruker IFS 66 FTIR spectrometer, equipped with an MCT detector. The samples, in the form of compressed self-supporting wafers, have been hosted inside a cell allowing in situ sample activation (done at 773 K in vacuo) and gas dosage to be made at liquid-nitrogen temperature. Raman spectra were recorded with a Renishaw micro-Raman system 1000 spectrometer equipped with a He−Cd laser emitting at $\lambda = 514$ nm (19445 cm^{-1}). The photons scattered by the sample were dispersed by a 2400 lines/mm grating monochromator and simultaneously collected on a CCD camera.

The optical properties of the samples (NVS-TiO_2 and I_2/NVS-TiO_2) have been studied by UV−vis spectroscopy in the reflectance mode (DRS) with a Perkin-Elmer Lambda 19 spectrometer in the 50 000-4000 cm^{-1} range and reported using the Kubelka−Munk function. TEM images were obtained on a Jeol 2000 EX electron microscope equipped with a top entry stage. Adsorption measurements were performed with a Micromeritics ASAP 2010 sorption analyzer. Surface areas have been obtained by N_2 adsorption at 77 K on all materials previously outgassed at 200 °C in vacuo.

For photocatalytic reactions the irradiation was carried out, in a Pyrex flask, on a 50 mL aqueous solution of 1×10^{-4} M methylene blue and 0.05 g of catalyst (NVS-TiO_2, I_2/NVS-TiO_2, and P25), directly exposed to the sunlight. At the end of the irradiation time a small amount of solution (2 mL) was taken, diluted with the same amount of deionized water, centrifuged for removing traces of catalyst, and than analyzed with UV−vis spectroscopy in the transmission mode with a Perkin-Elmer Lambda 19 spectrometer. In this way the relative photodegradation ability of I_2/NVS-TiO_2 and P25 materials can be directly compared.

Scheme 1. Pictorial Representation of Nanovoid-Structured TiO_2 (NVS-TiO_2 Material) Encapsulating the Products of the Combustion of the Organic Part of the Titanium Isopropoxide Molecule: CO_2 Molecules and Carbonates[a]

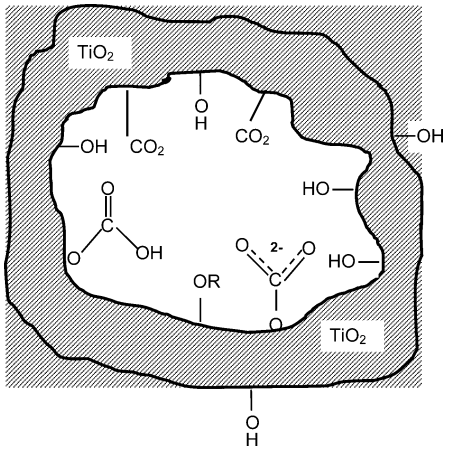

[a] Such nanovoids also contain internal surface OH groups. All these species cannot be perturbed by dosage of probe molecules like CO, as demonstrated by the IR experiment reported in Figure 3. The same pictorial representation holds for I_2/NVS-TiO_2 material with the only exception of the additional presence of $(I_2)_n$ adducts.

3. Results and Discussion

3.1. Nanovoid-Structured TiO_2: Assignment of Entrapped Molecular Species. The XRPD pattern of NVS-TiO_2 material, see Figure S1 in the Supporting Information, is characterized by the typical reflections of both anatase and rutile phase; see red and blue lines, respectively. The anatase phase is the most abundant one. No reflection belonging to other phases has been observed. Also the Raman spectrum, see Figure S2 in the Supporting Information, exhibits the typical modes of both anatase and rutile phases.[12] While the XRPD and Raman studies result in the classical pattern and spectra expected for a mixture of the two most common crystalline TiO_2 phases, the IR study highlights the presence of vibrational modes not belonging to titanium oxides. The full line in Figure 1 reports the IR spectrum, collected at room temperature, of NVS-TiO_2 material previously activated under dynamical vacuo (residual pressure $<10^{-4}$ Torr; 1 Torr = 133.3 Pa) at 773 K. For comparison, the IR spectrum of P25 catalyst, activated under the same conditions, is also reported as dotted line. The only vibrational features that could be ascribed to the TiO_2 phases observed in the IR spectrum of the NVS-TiO_2 material are the O−H modes of the surface Ti−OH groups. On P25 they appear as broad components with maxima at 3725 and at 3670 cm^{-1}, which frequencies reflect a different H-bond interaction with the surrounding.[7,8,40,50] In this region, as commented below, the IR spectrum of NVS-TiO_2, is dominated by two strong and well defined bands at 3705 and 3600 cm^{-1}, that are due to the combination modes of CO_2 molecules. As a consequence, the exact location of the surface Ti−OH groups cannot be assessed.

(49) Bersani, D.; Antonioli, G.; Lottici, P. P.; Lopez, T. *J. Non-Cryst. Solids* **1998**, *234*, 175−181.

(50) Morterra, C.; Bolis, V.; Fisicaro, E. *Colloids Surf.* **1989**, *41*, 177−188.

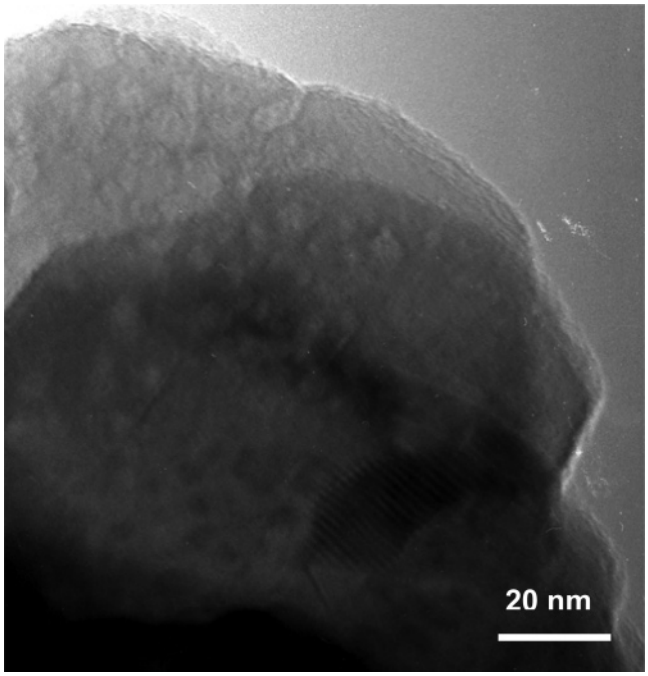

Figure 2. Typical TEM micrograph of the NVS-TiO_2 sample. Areas of higher electron transparency are clearly visible. Both external pores and internal nanovoids justify such a TEM micrograph.

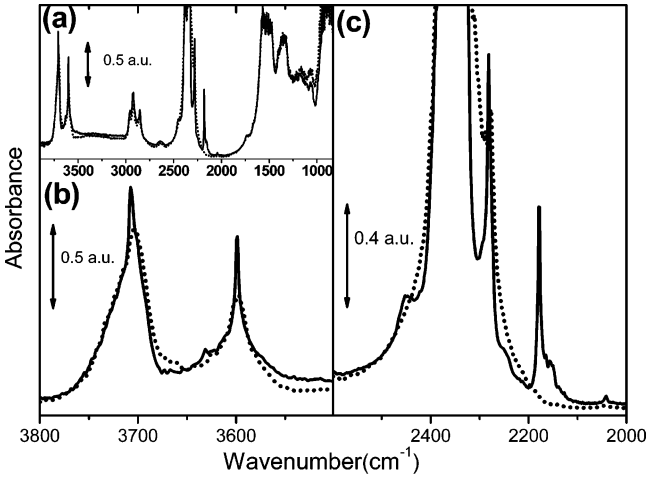

Figure 3. IR spectra, formally collected at liquid-nitrogen temperature, of NVS-TiO_2 sample prior (dotted line) and after (full line) interaction with CO: (a) whole mid-IR range; (b) zoom on the O−H stretching region; (c) zoom on the C−O and CO_2 stretching regions.

Other important features can be described as follows. (i) The sharp peak at 3600 cm^{-1} should also contain contributions from OH species in hydrogen carbonates;[51] see Scheme 1. (ii) The complex multiplet in the 2975−2840 cm^{-1} range is due to methyl and/or ethyl groups.[52,53] (iii) The huge absorption, saturating the spectrum at 2400−2270 cm^{-1}, is due to the asymmetric stretching of CO_2.[54] (iv) The huge and complex set of bands in the 1600−1000 cm^{-1} area, covers the region where carbonate and hydrogen carbonates species are expected.[31,51,55] The presence of CO_2 molecules has been further confirmed by the Raman experiment reported in the inset of Figure 1, where the typical mode of the symmetric stretching of CO_2,[54] is split into components at 1383 and at 1280 cm^{-1}, due the Fermi resonance with the overtone of the O═C═O bending mode (at 667 cm^{-1} in the gas phase: $2\delta = 1334$ cm^{-1}). This fact well explains the strong doublet at 3705 and 3600 cm^{-1} observed in the IR spectra (Figure 1) as the combination of the $\nu_{asym}(CO_2) + \nu_{sym}(CO_2)$. As for both IR and Raman features of CO_2, the absence of the rotovibrational contour as well as the red shift with respect to the gas-phase implies that we are dealing with adsorbed species. The important amount of CO_2 present on the sample can be appreciated by looking to the nonsaturated, sharp band at 2276 cm^{-1} due to the fraction of $^{13}CO_2$ naturally present in $^{12}CO_2$ (∼1%).

On the basis of the known properties of the surface species located on the external surface or on the meso- and micropores, isopropoxide groups and ethyl and/or ethyl groups, as well as weakly adsorbed molecules, such as CO_2, are expected to disappear after a sample pretreatment in air at 773 K. In particular the presence of adsorbed linear CO_2 (which is a weakly adsorbed species) even after thermal treatment at 773 K is definitely favoring the hypothesis that the TiO_2 prepared by following the procedure, illustrated before, is able to trap even highly volatile species. According to this evidence, we hypothesize that, during the calcinations process, nanovoids are formed inside the TiO_2 microcrystals, where the residues of the partial combustion of the organic part of the Ti precursor are trapped, as depicted in Scheme 1, and protected. For the time being, it is not possible to conclude about the mechanism of the partial combustion of the isopropoxide groups. During synthesis, the amount of molecular O_2 of the atmosphere that can be trapped inside the nanovoids is not able to justify the observed combustion products. The contribution of framework oxygen from TiO_2 is consequently hypothesized. Note that the presence of nanovoids inside the titania crystals prepared via the sol−gel method has been observed in the TEM investigation by Bersani et al.[49] Although no specific studies on this synthesis have been performed, we think that the formation of nanovoids could be explained in terms of the thermal aggregation of the pores present in the gel structure.

Our TEM study confirms the possible presence of nanovoids (see Figure 2). The TiO_2 crystals observed in such micrographs exhibit regions of significant contrast due to an important difference of material crossed by the beam. An important local decrease of the oxide phase crossed by the beam can be explained either in terms of external pores or by internal cavities or both. The IR and Raman investigations discussed above (Figure 1) and below (Figure 3) strongly suggest that the presence of nanovoids must be invoked. Of course this does not rule out the possible presence of external porosity, which has been evidenced by the small differences in the N_2 adsorption and desorption isotherms reported in Figure S4 of the Supporting Information. Note that the presence of external pores is probably the consequence of an incomplete incapsulation process.

A further confirmation of the fact that NVS-TiO_2 is a nanovoid-structured TiO_2 material comes from IR experiment

(51) Lavalley, J. C. *Catal. Today* **1996**, *27*, 377−401.
(52) Groppo, E.; Lamberti, C.; Bordiga, S.; Spoto, G.; Zecchina, A. *Chem. Rev.* **2005**, *105*, 115−183 and references therein.
(53) Groppo, E.; Lamberti, C.; Spoto, G.; Bordiga, S.; Magnacca, G.; Zecchina, A. *J. Catal.* **2005**, *236*, 233−244.
(54) (a) Garrone, E.; Bonelli, B.; Lamberti, C.; Civalleri, B.; Rocchia, M.; Roy, P.; Otero Arean, C. *J. Chem. Phys.* **2002**, *117*, 10274−10282. (b) Herzberg, G. *Molecular Spectra and Molecular Structure*; van Nostrand Reinhold: New York, 1950.
(55) Spoto, G.; Gribov, E. N.; Ricchiardi, G.; Damin, A.; Scarano, D.; Bordiga, S.; Lamberti, C.; Zecchina, A. *Prog. Surf. Sci.* **2004**, *76*, 71−146.

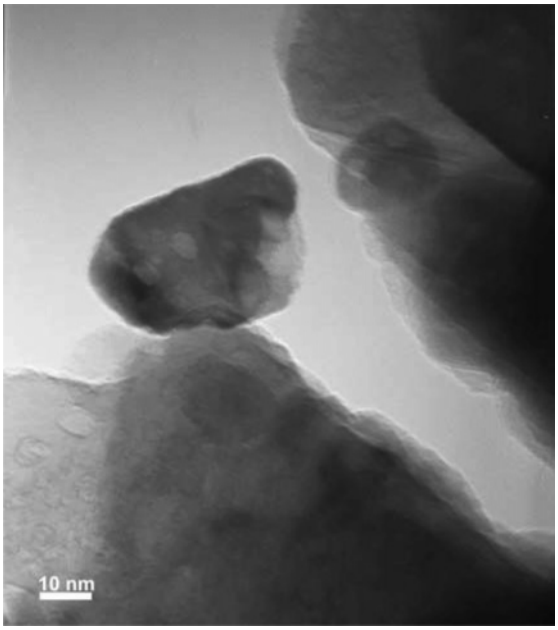

Figure 4. Typical TEM micrograph of I_2/NVS-TiO_2 sample. Areas of higher electron transparency, having linear dimensions in the 5−10 nm range, are clearly visible. Both external pores and internal nanovoids can result in this kind of TEM micrograph.

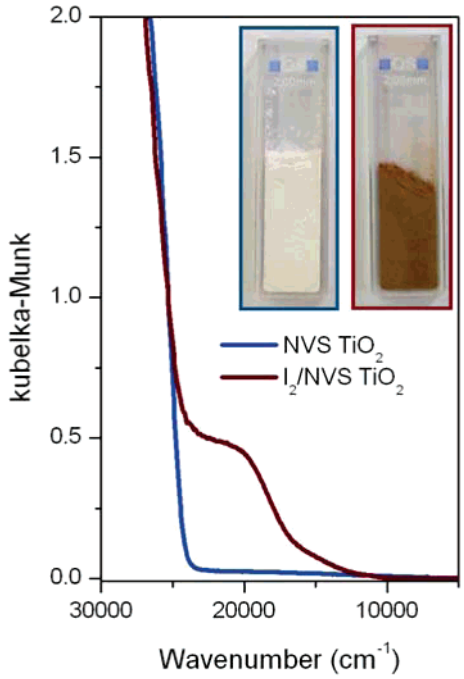

Figure 5. UV−vis DRS spectra of NVS-TiO_2 and I_2/NVS-TiO_2 samples, blue and brown lines, respectively. The insets report a color photograph of NVS-TiO_2 (left) and I_2/NVS-TiO_2 (right) samples.

reported in Figure 3, where the CO molecule has been used to probe the accessible surface species at liquid-nitrogen temperature.[52,56] From part a, reporting the whole Mid-IR region, it is evident that CO probe is unable to significantly perturb the IR manifestations of the surface species mentioned so far. More quantitative conclusions can be obtained by inspection of parts b and c of the same figure, reporting a zoom in the regions of O−H/CO_2 combination modes and C−O/C═O stretching modes, respectively. Only the minor fraction of the component at 3705 cm^{-1}, due to surface titanols, is eroded and red-shifted around 3670 cm^{-1}, due to the formation of Ti−OH···CO complexes (Figure 3b). The unperturbed fraction of the band at 3705 cm^{-1} is consequently ascribed to titanol species and CO_2 molecules hosted at the internal surfaces of the nanovoids that cannot be reached by CO probe. As the sharp component at 3600 cm^{-1} is mainly unaffected by CO dosage, it is due to the superimposition of the combination modes of CO_2 molecules with modes of molecular complexes grafted on the internal surfaces, such as hydrogen carbonate species (HO−CO_2^-);[51] see Scheme 1. Coming to the C−O/C═O stretching region, Figure 3c, the only significant difference observed upon CO adsorption at liquid nitrogen temperature is the appearance of the sharp band at 2178 cm^{-1} due to the C−O stretching of Ti^{4+}···CO complexes formed on the Lewis centers at the external surfaces.[7,50] The small differences observed in the huge absorption in the 2400−2270 cm^{-1} interval (due to CO_2 molecules adsorbed on the internal surfaces) are due to the decrease of temperature (about 20−30 K) reached upon dosing CO in the IR cell. A better heat transfer between the cold point and the sample is achieved by passing from vacuum to CO atmosphere.

3.2. $(I_2)_n$-Doped Nanovoid-Structured TiO_2. From the TEM, IR, and Raman investigations reported in the previous section, we could hypothesize that NVS-TiO_2 is a nanovoid-structured TiO_2 material and that molecular species can be trapped and protected inside them. Furthermore, the Ti−OR species confer to the internal surfaces a reducing character. This facts suggest the possibility to modify the sample synthesis with the aim of including some dye molecule inside the crystal nanovoids,[4] in order to obtain a TiO_2-based material able to absorb light in the visible region of the electromagnetic spectrum. In this study, iodine has been chosen as the dye. The advantages of this choice are 3-fold: (i) The high solubility in the titanium isopropoxide used as precursor allows a straightforward synthesis. (ii) The boiling point (around 184 °C) guarantees an easy elimination of the fraction of iodine non encapsulated inside the nanovoids. (iii) The reducing character of the environment afforded by the Ti−OR groups in the nanovoids is preventing further oxidation of iodine during the thermal treatments.

Iodine insertion in the synthesis batch does not modify the morphology of the TiO_2 crystals, as suggested by the TEM investigation reported in Figure 4, compared with Figure 2. TEM micrographs of the crystals of the I_2/NVS-TiO_2 material exhibits areas of higher electron transparency, having linear dimensions in the 5−10 nm range. As already discussed above for the NVS-TiO_2 case, both external pores and internal nanovoids can be hypothesized. The presence of the former has been evidenced by 77 K N_2 adsorption/desorption experiments (see Figure S4 in the Supporting Information), while the presence of the latter is needed to explain the vibrational results reported in Figures 1 and 3.

XRPD study, see Figure S3 of the Supporting Information, indicates that the main differences between NVS-TiO_2 and I_2/NVS-TiO_2 materials consist of a small modification of the anatase/rutile ratio, slightly higher in the doped sample.

Insertion of iodine successfully causes the red shift of the material absorption, which is a red/brown powder, while the parent NVS-TiO_2 is a white one; compare the right and the left

(56) Zecchina, A.; Scarano, D.; Bordiga, S.; Spoto, G.; Lamberti, C. *Adv. Catal.* **2002**, *46*, 265−397.

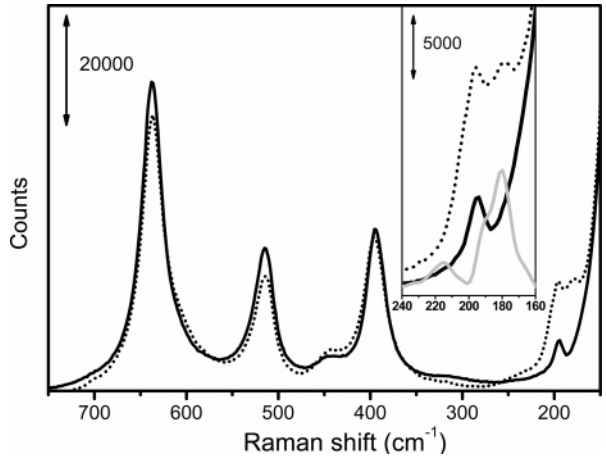

Figure 6. Raman spectra of NVS-TiO_2 and I_2/NVS-TiO_2 samples, dotted and full lines, respectively. The inset reports a magnification of the low Raman shift region, where the modes of $(I_2)_n$ adducts are expected at 179 cm^{-1}. The gray curve reports the Raman spectrum of iodine bulk.

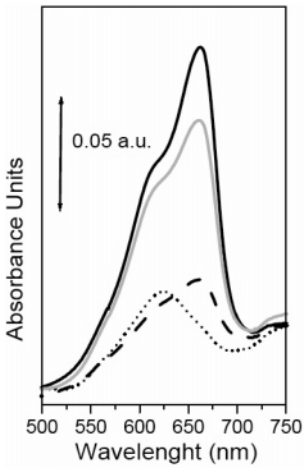

Figure 7. Transmission UV−vis spectra of methylene blue (full line) methylene blue/NVS-TiO_2 catalysts (gray curve), methylene blue/I_2/NVS-TiO_2 catalyst (dashed curve), and methylene blue/P25 catalyst (dotted curve) after exposure for 2 days to sunlight (corresponding to about 24 h of overall illumination).

insets in Figure 5. The quantification of this phenomenon is given in the main part of Figure 5, reporting the UV−vis spectra of both NVS-TiO_2 and I_2/NVS-TiO_2 materials; see blue and brown curves, respectively. A broad absorption band appears in the interval between 25 000 cm^{-1} (400 nm) and 15 000 cm^{-1} (667 nm), i.e., covering the whole visible range, is clearly present in the spectrum of I_2/NVS-TiO_2 reported in Figure 5. This band is centered around 20 000 cm^{-1} (500 nm). This is the spectral range where iodine absorbs.[57,58]

The Raman spectra of NVS-TiO_2 and I_2/NVS-TiO_2 materials (full and dotted curves in Figure 6) are dominated by the strong bands due to both anatase and rutile phases; see also Figure S2 of the Supporting information. The only significant difference between the two spectra (see inset) consists in the band at 179 cm^{-1} and in a shoulder around 215 cm^{-1}, both appreciable on the right and left side of the anatase mode at 196 cm^{-1}, respectively. Bulk iodine exhibits the A_g (strong) and the B_{3g} (medium) modes at 180 and 188 cm^{-1}, respectively.[59] See also the gray spectrum reported in the inset of Figure 6. The I−I stretching of the I_2 molecule in the gas phase occurs at 213 cm^{-1}.[58,60] Note that, in the Raman spectrum of bulk iodine (gray spectrum reported in the inset), the band at 215 cm^{-1}, gaining in intensity with increasing laser power, is due to I_2 molecules sublimating from the solid as a consequence of the heating power of the light source. Consequently we conclude that iodine is present in our sample mainly as $(I_2)_n$ adducts encapsulated in the TiO_2 nanocavities (mode at 179 cm^{-1}). A minor fraction of I_2 molecules in the gas phase is also present under the Raman experimental conditions (shoulder at 215 cm^{-1}). It is not possible to discriminate whether I_2 molecules are present inside the TiO_2 nanovoids in the absence of the laser source or not.

3.3. Effect of Iodine-Loading on the Photocatalytic Activity: Preliminary Results. The data reported in section 3.2 show that I_2/NVS-TiO_2 is a nanovoid-structured TiO_2 material able to absorb light in the whole visible interval of the electromagnetic spectrum and that the origin of this absorption is the presence of $(I_2)_n$ adducts encapsulated in the nanocavities. Now, the crucial point is to evaluate whether the energy trapped by the $(I_2)_n$ adducts upon visible light absorption can be transferred to the TiO_2 bulk to create an electron−hole pair, first, and then to the external surface of the oxide particles where photocatalysis can take place.

The photocatalytic ability of I_2/NVS-TiO_2 and NVS-TiO_2 materials has been tested in the degradation of methylene blue. Aqueous solutions of methylene blue have been contacted with I_2/NVS-TiO_2, with NVS-TiO_2, and with P25 photocatalysts, while a fourth flask has been prepared without catalyst as a blank sample to take into account the self-degradation of the molecule under visible light. The four flasks have been simultaneously exposed to the direct sunlight for 2 days, corresponding to about 24 h of overall illumination. Figure 7 reports the UV−vis spectra of the four specimens after the irradiation process. In all cases the electronic transitions of the methylene blue molecule at 664 nm (15 000 cm^{-1}) and 612 nm (16 340 cm^{-1}) are clearly visible.[48] Note that an analogous experiment performed for 2 days in the dark by contacting an aqueous solution methylene blue with both I_2/NVS-TiO_2 and NVS-TiO_2 materials resulted in an almost unappreciable degradation.

The positive role of both I_2/NVS-TiO_2 and P25 materials in the photodegradation is evident. Also the NVS-TiO_2 material is active in the photodegradation of methylene blue, but with a much lower efficiency, due to the significantly lower surface area. The degradation efficiency of I_2/NVS-TiO_2 and P25 photocatalysts is comparable as the bands of the electronic modes of methylene blue are reduced in absorbance units by a factor of about 3 in both cases. The huge difference in the surface area of the two materials (3.85 vs and 60 m^2 g^{-1} for I_2/NVS-TiO_2 and P25, respectively) implies that there is more than 1 order of magnitude of difference in the number of surface titanol groups where the photocatalytic degradation of methylene blue can occur. The combination of these two observations implies that the surface-specific efficiency in converting solar photons into electron−holes pairs, able to reach the external

(57) Gray, R. I.; Luckett, K. M.; Tellinghuisen, J. *J. Phys. Chem. A* **2001**, *105*, 11183−11191.
(58) Stoimenov, P. K.; Zaikovski, V.; Klabunde, K. J. *J. Am. Chem. Soc.* **2003**, *125*, 12907−12913.
(59) Anderson, A.; Sun, T. S. *Chem. Phys. Lett.* **1970**, *6*, 611−616.
(60) Howard, W. F., Jr.; Andrews, L. *J. Raman Spectrosc.* **1974**, *2*, 447−462.

titanols, is about 1 order of magnitude greater in I_2/NVS-TiO_2 material then in the standard P25 photocatalyst.

The activity of both NVS-TiO_2 and P25 photocatalysts is due to the small fraction of sun light in the UV region (about 5%), able to generate an electron−hole pair in TiO_2.[1,6,40] The important enhancement of the activity of I_2/NVS-TiO_2 photocatalyst, with respect to that of NVS-TiO_2, is associated with the presence of $(I_2)_n$ dyes encapsulated and protected inside the nanovoids. According to the literature,[6,10,11,35,40,61−63] the dye $(I_2)_n$ absorbing a visible photon is promoted into an excited electronic state $(I_2)_n$*, from which an electron can be transferred into the conduction band of the semiconductor (TiO_2) according to eqs 2 and 3:

$$(I_2)_n + h\nu \rightarrow (I_2)_n^* \quad (2)$$

$$(I_2)_n^* + TiO_2 \rightarrow [(I_2)_{n\bullet}]^+ + TiO_2\,(e^-) \quad (3)$$

Once the electron reaches the TiO_2 conduction band, it is able to move until attaining the external surface, where the photodegradation process can occur according to the standard mechanism. The efficiency of reaction 2 is high, as we have used a dye able to absorb visible photons, while the efficiency of the reaction 3 depends upon the quantum yield of the dye/semiconductor redox process.[6,35] Transferring the model of band alignment, well established in the field of solid-state physics applied to semiconductor heterostructures,[64−70] to the field of photocatalysis, Usseglio et al.[40] have recently suggested that the quantum yield of reaction 3 is high when there is a good match between the energy position of the dye* level and the bottom of the semiconductor conduction band; see the scheme reported in Figure 10 of that work. Note that this mechanisms is the working principle of the Grätzel-type or dye-sensitized cells.[6,71−77] The results reported in Figure 7 imply that the energy level of the excited electron in the $(I_2)_n$* molecule should be very close, or slightly above the bottom of the TiO_2 conduction band, thus guaranteeing a good quantum efficiency of reaction 3.

4. Conclusions

Combined IR, Raman, and TEM study indicates that the reported synthesis of titanium oxide via a sol−gel route using titanium isopropoxide as precursor results in a nanovoid-structured TiO_2 material. XRPD and Raman indicate the presence of both anatase and rutile phases. IR and Raman show that the surfaces of internal cavities are populated by the partial oxidation products (hydrogen carbonates, adsorbed carbon dioxide, and residual OR groups) of the organic part of the precursor that are not perturbed by the dosage of probe molecules. Such internal surface species are protected as they are encapsulated during thermal treatments at 773 K.

Addition of iodine in the synthesis procedure results in a new nanovoid-structured titanium oxide with the same morphology but able to absorb light in the whole visible interval of the electromagnetic spectrum. UV−vis and Raman spectra prove that the origin of this absorption is the presence of $(I_2)_n$ adducts encapsulated in the nanocavities. The photoactivity of I_2/NVS-TiO_2 in the photodegradation of methylene blue using sunlight is comparable to that of the P25 commercial TiO_2 photocatalyst. The activity of I_2/NVS-TiO_2 implies an electron injection from dye* to either the TiO_2 conduction band or some titanium-localized acceptor, followed by migration of the injected electron to the surface where it reduces the adsorbed organic molecules. Considering that the surface area of I_2/NVS-TiO_2 is smaller than that of P25 by 1 order of magnitude, we concluded that when sunlight is used, the surface specific efficiency of this process is about 10 times higher than that of the P25. This result encourages the synthesis of new iodine-doped nanovoid-structured TiO_2 material characterized by an higher surface area.

Acknowledgment. Prof. G. Spoto is acknowledged for the TEM study and fruitful discussion. We are indebted to Prof. G. Busca for a critical discussion on the IR spectra reported here. We are indebted to the authors of ref 26 for having kindly communicated their results to us prior to publication. The financial support of the NATO program for security through science "Science for Peace Proposal" (SFP No. 981476) is gratefully acknowledged. This research has also been partially supported by the Italian MIUR through the PRIN 2005 project coordinated by Prof. G. Pacchioni.

Supporting Information Available: Powder XRD and Raman spectra of both NVS-TiO_2 and I_2/NVS-TiO_2 materials and volumetric N_2 adsorption/desorption isotherms at 77 K of the I_2/NVS-TiO_2 catalyst. This material is available free of charge via the Internet at http://pubs.acs.org.

JA066083M

(61) Serpone, N.; Lawless, D.; Khairutdinov, R.; Pelizzetti, E. *J. Phys. Chem.* **1995**, *99*, 16655−16661.
(62) Liu, Y.; Dadap, J. I.; Zimdars, D.; Eisenthal, K. B. *J. Phys. Chem. B* **1999**, *103*, 2480−2486.
(63) Kim, S.; Choi, W. *J. Phys. Chem. B* **2005**, *109*, 5143−5149.
(64) Van de Walle, C. G.; Martin, R. M. *Phys. Rev. B* **1986**, *34*, 5621−5634.
(65) Van de Walle, C. G.; Martin, R. M. *Phys. Rev. B* **1987**, *35*, 8154−8165.
(66) Bastard, G.; Brum, J. A.; Ferreira, R. *Solid State Phys.: Adv. Res. Appl.* **1991**, *44*, 229−415.
(67) Franciosi, A.; Van de Walle, C. G. *Surf. Sci. Rep.* **1996**, *25*, 1−140.
(68) Margaritondo, G. *Rep. Prog. Phys.* **1999**, *62*, 765−808.
(69) Lamberti, C. *Comput. Phys. Commun.* **1996**, *93*, 53−81.
(70) Lamberti, C. *Surf. Sci. Rep.* **2004**, *53*, 1−197.
(71) Oregan, B.; Grätzel, M. *Nature* **1991**, *353*, 737−740.
(72) Cherian, S.; Wamser, C. C. *J. Phys. Chem. B* **2000**, *104*, 3624−3629.
(73) Nagai, H.; Segawa, H. *Chem. Commun.* **2004**, 974−975.
(74) Frank, A. J.; Kopidakis, N.; van de Lagemaat, J. *Coord. Chem. Rev.* **2004**, *248*, 1165−1179.
(75) Schwarzburg, K.; Ernstorfer, R.; Felber, S.; Willig, F. *Coord. Chem. Rev.* **2004**, *248*, 1259−1270.
(76) Campbell, W. M.; Burrell, A. K.; Officer, D. L.; Jolley, K. W. *Coord. Chem. Rev.* **2004**, *248*, 1363−1379.
(77) Duncan, W. R.; Stier, W. M.; Prezhdo, O. V. *J. Am. Chem. Soc.* **2005**, *127*, 7941−7951.